Mass transfer characteristics of a continuously operated hollow-fiber membrane contactor and stripper unit for CO2 capture

Nieminen Harri, Järvinen Lauri, Ruuskanen Vesa, Laari Arto, Koiranen Tuomas, Ahola Jero

DOI: 10.1016/j.ijggc.2020.103063

Mass transfer characteristics of a continuously operated hollow-fiber membrane contactor and stripper unit for CO_2 capture

H. Nieminen*[1], L. Järvinen[2], V. Ruuskanen[2], A. Laari[1], T. Koiranen[1], J. Ahola[2]

1 Lappeenranta-Lahti University of Technology, Laboratory of Process Systems Engineering, P.O. Box 20, FI-53851 Lappeenranta, Finland

2 Lappeenranta-Lahti University of Technology, Laboratory of Control Engineering and Digital Systems, P.O. Box 20, FI-53851 Lappeenranta, Finland

Abstract

Mass transfer performance of a polypropylene hollow-fiber membrane contactor as part of a continuously operated CO_2 capture unit with amino acid salt (potassium glycinate) absorbent and vacuum solvent regeneration was studied. The effects of key operating parameters on the absorption mass transfer characteristics were explored. Without vacuum stripping, absorption rate was found to be limited by low CO_2 desorption efficiency from the loaded absorbent solution in the stripping unit, resulting in high solvent CO_2 loadings and limited chemical absorption rates. Introduction of vacuum stripping greatly improved desorption performance, resulting in improved steady-state absorption performance. The overall mass transfer coefficient increased at higher stripping temperatures and lower vacuum pressures in the range of 60-80 °C and 300-800 mbar (abs). The overall mass transfer coefficient increased with increasing liquid flow rate, and the highest value reached was $1.8 \cdot 10^{-4}$ m s^{-1}. The individual mass transfer coefficients in absorption were calculated based on mass transfer correlations and experimental data, including estimation of the enhancement factor for chemical absorption. The overall mass transfer resistance was found to be dominated by the liquid-side resistance, at almost 90 % of the total resistance. The estimated membrane mass transfer coefficient was low compared to a theoretical value assuming non-wetted operation, suggesting potential partial wetting of the membrane. Stable performance of the unit and the membrane contactor was demonstrated during a stability test with over 30 hours of operation.

Keywords

CO_2 capture, membrane contactor, vacuum, stripping, desorption, amino acid salt, potassium glycinate

Declarations of interest: none

1. Introduction

The continuously increasing atmospheric carbon dioxide (CO_2) concentration resulting from growing global CO_2 emissions has been linked to detrimental climatic effects [1]. Development of carbon capture technologies for the separation of carbon dioxide both from point emission sources and directly from the atmosphere could provide a partial solution for the mitigation of CO_2 emissions [2]. Furthermore, the utilization of captured CO_2 by chemical conversion could provide a fossil-free route to various valuable fuel or chemical products [3].

The established technology for the capture of CO_2 from flue gases or process streams is based on chemical absorption in columns using basic solutions such as aqueous amines, most commonly monoethanolamine (MEA) [4, 5]. The process consists of absorption of CO_2 into the solution followed by solvent regeneration and release of CO_2 by heating of the CO_2-loaded solution [6]. The solvent regeneration stage requires a significant amount of heat, which constitutes the main operating cost of the overall capture process [5]. Thus, reduction of the energy consumption is a major motivation for the development of alternative CO_2 capture processes. Another objective is to decrease the desorption temperature level, which would enable the usage of waste heat streams, solar thermal and heat pumps for the generation of required heat energy. Such alternatives include the utilization of alternative absorbents [7, 8, 9], or alternative processes based on absorption [10] or membrane separation [11].

Alternative for columns is the use of membrane gas-liquid contactors, where CO_2 is absorbed to the chemical absorbent via mass transfer through a porous, non-selective membrane [12, 13]. A major advantage of membrane contactors compared to conventional absorption equipment is the significantly higher interfacial area per unit volume offered by the membrane hollow fiber configuration [14, 15]. The interfacial area remains constant regardless of the operating conditions which allows highly flexible operation and independent adjustment of the gas and liquid flow rates. In addition, the module orientation can be freely selected, and simple linear scale-up is facilitated by increasing the number of modules and the total membrane area.

A disadvantage of membrane contactors is the added mass transfer resistance caused by the membrane. In order to minimize this resistance, microporous polymeric materials such as polypropylene (PP) and polytetrafluoroethylene (PTFE) are commonly employed [13]. The membrane has to be hydrophobic in order to resist wetting by the aqueous absorbent, as mass transfer is severely limited if the membrane operates in wetted mode [16]. Compatibility of the membrane material and the absorbent is vital for preventing membrane wetting. As cost-effective PP membranes have been found to be wetted by common amine absorbents during longer contact times [17, 18, 19], the use of alternative absorbents in membrane contactors has found interest. Aqueous amino acid salts offer comparable CO_2 absorption rates and capacities compared to amine solutions combined with a high surface tension and low wetting tendency [20, 21, 22]. In addition, the ionic absorbents possess low volatility and toxicity. An example of an amino

acid salt considered for membrane contactors is potassium glycinate [21, 23, 24, 25], formed by neutralization of the amino acid glycine with potassium hydroxide.

The present study analyses the continuous absorption and desorption of CO_2 utilizing a membrane contactor with the potassium glycinate absorbent. Reports on such complete, continuous processes are relatively scarce as the majority of previous literature has focused primarily on the absorption stage. However, some reports of complete capture processes based on membrane contactors in the laboratory and pilot scale are available [26, 27, 22, 28, 29, 30, 31]. These processes are generally based on the combination of a membrane contactor for absorption with a conventional stripper for desorption. The use of membrane contactors for CO_2 stripping would be interesting as the same advantages found in the absorption stage could be realized also at the solvent regeneration stage. However, a major challenge is the requirement for membrane stability at elevated temperatures. Instead of low-cost polymeric membranes, membranes with a more limited availability and higher cost are generally required for stable performance under desorption conditions [32, 33, 34, 35].

The application of vacuum for CO_2 stripping has been suggested for lowering the solvent regeneration temperature and the corresponding energy consumption [36]. Decreasing the regeneration temperature would also serve to increase the applicability of common membrane materials incapable of withstanding higher operating temperatures. Vacuum desorption of CO_2 from various amine solutions using PP hollow fiber contactors has been demonstrated [37, 38]. For reference, Fang et al. [37] performed desorption at pressures of 10-35 kPa and temperatures of 40-70 °C, showing the potential for significant decreases in the regeneration temperature. The vacuum regeneration performance of potassium glycinate has been found comparable to amines [39], suggesting potential for utilizing amino acid salts in such a process.

This work characterises the CO_2 capture performance of a continuously operated unit combining absorption in a membrane contactor and solvent regeneration utilizing vacuum. It is in continuation of a previous report which focused on the design and operation of the unit and presented initial findings concerning the absorption/desorption performance and energy consumption [40]. The present report provides a more detailed mass transfer analysis of the membrane contactor in a CO_2 absorption/desorption process during steady-state operation. The aim is to assess the effect of key process parameters on the mass transfer performance of the membrane module, as primarily measured by the gas-side overall mass transfer coefficient. In addition, the gas, membrane and liquid individual mass transfer resistances are evaluated from mass transfer correlations and measured absorption data. In addition, stable performance is demonstrated during a stability test with over 30 hours of operation. A number of data points, as referenced, are reproduced from the previous publication.

2. Experimental

2.1. CO_2 capture unit

The continuously operated CO_2 capture unit consists of a hollow fiber membrane module as the absorber, a reaction vessel acting as a stripper and a buffer tank for the absorbent solution, and pumping and temperature control equipment for maintaining absorbent liquid circulation at controlled temperatures. A flowsheet of the unit is presented in Figure 1. The same unit was first described in a previous publication [40]. The membrane surface area of the PP hollow fiber membrane module (Liqui-Cel™ 2.5 x 8 Extra-Flow, supplied by 3M) is 1.4 m^2. In the membrane module, the absorbent flows upwards inside the hollow fibers (lumen side) while the inlet gas flows countercurrent on the shell side.

The inlet gas consists of nitrogen or air mixed with CO_2 (10 % v/v unless stated otherwise) for a simulated flue gas composition, with gas flows controlled by mass flow controllers (Bronkhorst EL-FLOW Select, accuracy ±0.5% reading, ±0.1% full scale). The CO_2 concentration of the inlet gas is verified by an IR-analyzer analyzer (GMP251 probe, ±0.2 % CO_2, and Indigo 201 transmitter, both supplied by Vaisala). The gas pressure is controlled by a back-pressure controller (Bronkhorst EL-PRESS, ±0.1% reading, ±0.5% full scale) located at the membrane gas outlet. The pressure at the gas outlet is maintained at 0.1 bar below the liquid inlet pressure in order to avoid wetting of the membrane by the absorbent solution. The CO_2 concentration of the outlet gas is measured by a separate IR-analyzer (Vaisala GMP251 probe and Indigo 201 transmitter).

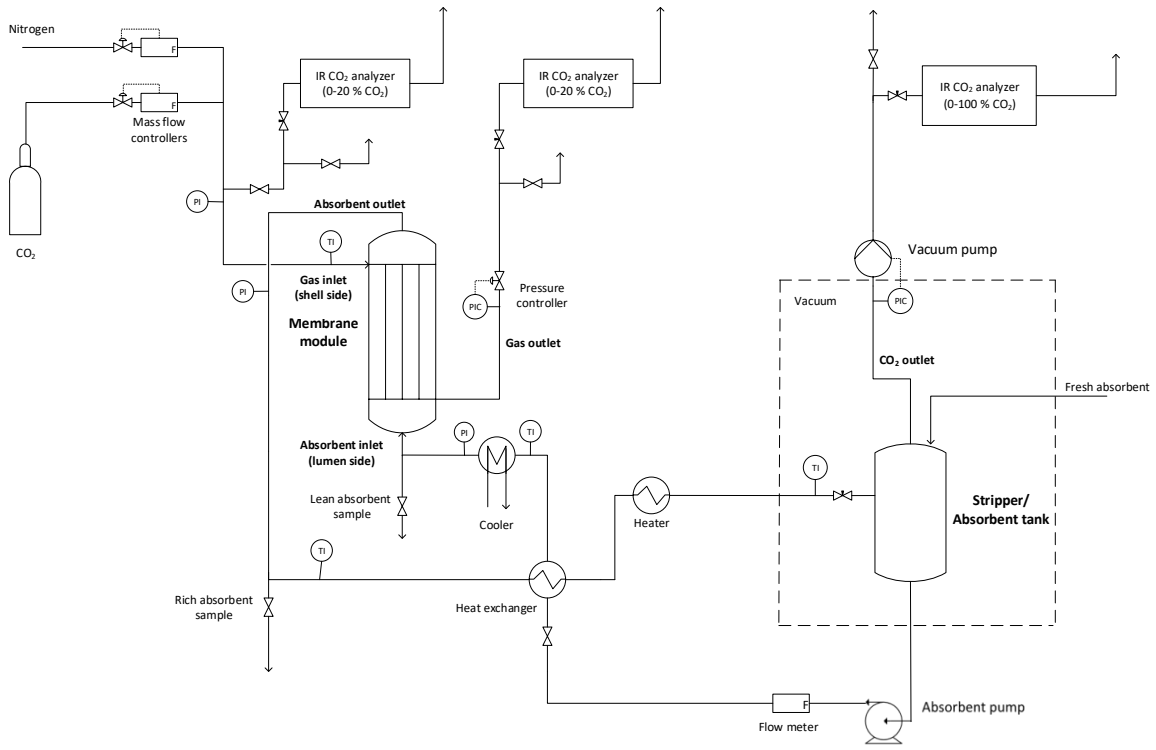

Figure 1 Flowsheet of the experimental CO_2 capture unit [36].

Liquid is pumped through the system by a magnetic drive gear pump (Pulsafeeder Eclipse E12) and the liquid flow rate is measured by a flow meter (Litre Meter LMX.48, ±2 % reading) located directly after the pump. The CO_2-lean absorbent pumped at the regeneration temperature (60-80 °C) is first cooled in a plate heat exchanger (Alfa Laval, 1.6 m^2) in which heat is transferred to the cold absorbent exiting the membrane module. The liquid is then cooled to the absorption temperature (10-30 °C) in another plate heat exchanger (Alfa Laval, 0.2 m^2) with cooling water as the cold fluid. The temperature of the cooling water is controlled by a circulating cooler (Lauda Variocool VC5000, ±0.05 °C). After flowing through the membrane module, the CO_2-rich absorbent is first heated in the heat exchanger and then heated to the regeneration temperature in a hot water heater. The liquid pressure on the absorption side is adjusted by a manual needle valve located before the stripper.

For use of vacuum in solvent regeneration, the gas outlet from the stripper vessel is connected to a vacuum pump (Vacuubrand MZ 2C NT) via an automatic vacuum control unit (Vacuubrand CVC-3000, ±1 mbar). The outlet gas from the vacuum pump flows to an IR CO_2-analyzer (CO2Meter CM-0052, ±3 % reading, ± 0.5 % full scale) with a 0-100 % v/v measuring range. In addition to CO_2, the analyzer measures the oxygen concentration with a 0-100 % v/v measuring range.

The control and data acquisition system is implemented with LabVIEW software. Data acquisition system (NI cDAQ-9189) is used for data gathering and analog control signals output. 4-20 mA analog input signals are measured with NI 9208 module (accuracy ±0.76 % reading), and 4-20 mA analog output module (NI

9266, ±0.76 % reading, ±1.4 % full scale) is used to set reference values for the process units. The system includes online measurement of the electricity consumed by the liquid and vacuum pumps, and calculation of the heat energy consumed in heating of the absorbent to the regeneration temperature, based on the measured flow rate and temperature difference. The electrical supply power is measured with a Sentron PAC3200 (±0.5 % reading) three-phase power analyzer equipped with MAK 62/W 25/1A current transformers.

2.2. Chemicals

The potassium glycinate absorbent was prepared by neutralization of glycine (Sigma-Aldrich, >99%) with an equimolar amount of potassium hydroxide (Sigma-Aldrich, >85 w-%) in purified water. The solutions were prepared in a glass vessel equipped with a cooling water jacket. The concentration of all solutions was verified by potentiometric titration (Mettler-Toledo T50) using 1 M hydrochloric acid. The concentration of all solutions was within 1% of the nominal concentration. In the CO_2 capture experiments, the feed gas consisted of technical grade nitrogen (>99.5 %) or ambient air mixed with CO_2 from a gas cylinder (>99.99 %). 1 M hydrochloric acid and methyl red (5% solution in ethanol) were used in the titrimetric CO_2-loading analysis of the liquid absorbent samples.

2.3. Procedure

The equipment was filled with 6 l of the absorbent solution; using this volume, the liquid level in the absorbent vessel was approximately half the vessel height. The system was started by flowing nitrogen through the membrane contactor, after which the liquid flow was started. The flows of CO_2 and nitrogen were then adjusted to reach the desired gas flow rate and composition. The CO_2 concentration (vol%) of the feed gas was verified by directing a portion of the flow to the IR-analyzer. Following this verification, the flow of feed gas to the analyzer was closed in order to measure the exact flow rate being delivered to the membrane contactor. The heater and cooler were turned on to adjust the liquid temperature during absorption and desorption. The pressure of the liquid entering the membrane module was adjusted using the manual needle valve located before the desorption vessel. In the vacuum desorption runs, the vacuum pump was switched on and the vacuum pressure was controlled by the vacuum control valve.

Unless otherwise stated, all experimental data was collected under steady-state conditions, as indicated by stable operating conditions (temperatures, flow rates, pressures) together with a stable CO_2 concentration at the outlet of the membrane module (measured by the IR-analyzer). Depending on the process parameters, the time required to achieve steady-state was above 8 hours after fresh absorbent was introduced, due to the slow increase in the CO_2-loading of the circulating liquid. Following a change in the experimental conditions without absorbent replacement, the new steady-state was generally reached within 2 hours.

The steady-state data were collected for periods of approximately 1 min in the LabView environment, and the final results were calculated as the average values during the sampling period. Liquid samples were

also collected under steady-state conditions to analyze the CO_2 loading of the absorbent (mol CO_2 absorbed per mol of potassium glycinate). One rich solvent sample (collected after the membrane module) and one lean solvent sample (collected before the membrane module) were collected. Each sample was analyzed three times by titration with 1 M hydrochloric acid with methyl red indicator with the volume of released CO_2 measured. This analysis was performed using a specifically designed Chittick-apparatus (Soham Scientific). The repeatability of the triplicate measurements was generally within 1.5% (relative standard deviation) with a maximum accepted deviation of 3.0%.

A summary of the main operating parameters is presented in Table I. The experimental plan consisted of varying the absorbent flow rate, the CO_2 concentration in the feed gas, and the absorption and desorption temperatures. In the vacuum desorption experiments, the vacuum pressure was also varied. The repeatability of the experiments was checked by performing a series of repeat runs at one operating point. The standard error of the mean was calculated for each measured or calculated result observed in these repeat runs and multiplied by a factor of 2 for a 95% confidence interval. The same confidence interval is assumed to hold for all data points. These confidence intervals are presented as error bars in the relevant figures.

Table I Main operating parameters in the experiments.

Membrane surface area: 1.4 m^2
Absorbent concentration: 1 M
Absorbent flow rate: 0.75-1.5 l min^{-1} (superficial velocity 0.03-0.06 m s^{-1})
Feed gas CO_2 concentration: 5-15 vol-% (CO_2 partial pressure 5.75-17.25 kPa)
Feed gas flow rate: 5 l min^{-1} (superficial velocity 0.05 m s^{-1})
Absorption temperature: 10-30 °C
Desorption temperature: 60-80 °C
Desorption vacuum pressure: 300-800 mbar (abs)

2.4. Theory and calculations

The overall mass transfer process in a membrane gas-liquid contactor consists of diffusion of CO_2 from the bulk gas phase to the gas-membrane interface, through the membrane pores to the membrane-liquid interface, and to the bulk liquid followed by chemical and/or physical absorption. The process can be described by the resistance-in-series model using the individual mass transfer coefficients for the gas, liquid and membrane phases. The gas-side overall gas-phase mass transfer coefficient is given by the following expression [41, 42]:

$$\frac{1}{K_{\mathrm{G}}} = \frac{1}{k_{\mathrm{G}}} + \frac{1}{k_{\mathrm{M}}} + \frac{1}{mk_{\mathrm{L}}E} \quad (1)$$

Where k_{G}, k_{M}, and k_{L} are the gas, membrane and liquid mass transfer coefficients, respectively, m is the distribution coefficient of CO_2 between gas and liquid phases (dimensionless Henry's constant), and E is the enhancement factor caused by chemical reaction defined as the ratio of the absorption flux in the presence of reaction and the flux with only physical absorption taking place:

$$E = \frac{N_{\mathrm{chem}}}{N_{\mathrm{phy}}} \quad (2)$$

Where N refers to the CO_2 flux through the membrane.

In aqueous solution, amino acid salts formed by the neutralization of amino acids by a strong base are present in the amine form. The amino acid salts are weakly basic, e.g. the pK_a of potassium glycinate is 9.67 [23]. Similarly to aqueous alkanolamines, chemical absorption of CO_2 by aqueous amino acid salts is considered to take place by the zwitterion mechanism, where dissolved CO_2 and the amino acid salt form a zwitterion intermediate (Eq. 3), which is then deprotonated by a base present in solution (Eq. 4) to form carbamate [43]. CO_2 may also react with hydroxide ions present in solution, forming bicarbonate (Eq. 5). The kinetics of CO_2 absorption is controlled by the carbamate formation reaction. The ratio of carbamate and bicarbonate formed varies with the type of amino acid salt, the reaction conditions, and the CO_2 loading of the solution [44, 45].

$$\mathrm{H_2NCH_2COOK^+ + CO_2 \rightleftharpoons {}^-OOC^+H_2NCH_2COO^-K^+} \quad (3)$$

$$\mathrm{{}^-OOC^+H_2NCH_2COO^-K^+ + B_i \rightleftharpoons {}^-OOCHNCH_2COO^-K^+ + B_iH^+} \quad (4)$$

$$\mathrm{CO_2 + OH^- \rightarrow HCO_3^-} \quad (5)$$

Where $\mathrm{B_i}$ refers to H_2O, OH^-, or the amino acid salt, all capable of deprotonating the zwitterion. The overall forward rate for the chemical absorption of CO_2 can be given by [46]

$$R_{\mathrm{CO_2}} = \frac{k_1[\mathrm{CO_2}][\mathrm{A}]}{1 + \frac{k_{-1}}{\sum k_{B,i}[\mathrm{B}_i]}} \quad (6)$$

Where $[\mathrm{A}]$ is the amino acid salt concentration, and the kinetic constants k_1 and k_{-1} refer to the forward and reverse reactions described by Eq. 3. $\sum k_{B,i}[\mathrm{B}_i]$ includes the contribution of bases B_i in the removal of protons (Eq. 4), with $k_{B,i}$ referring to the deprotonation rate constant for the corresponding bases B_i.

The CO_2 flux was calculated from the experimental data using the following expression:

$$N = \frac{\dot{n}_{\mathrm{CO_2,in}} - \dot{n}_{\mathrm{CO_2,out}}}{A} \quad (7)$$

Where N is the flux , $\dot{n}_{\mathrm{CO_2,in}}$ and $\dot{n}_{\mathrm{CO_2,out}}$ are the CO_2 molar flows in the inlet and outlet gas, respectively, and A is the membrane outer surface area in the module. The molar CO_2 flows were calculated from the

mass balance over the membrane module, assuming nitrogen and oxygen as inert gases with no absorption.

The CO_2 capture efficiency, i.e. the fraction of CO_2 absorbed from the feed gas, was calculated from

$$\eta_{\mathrm{abs}} = \frac{\dot{n}_{\mathrm{CO_2,in}} - \dot{n}_{\mathrm{CO_2,out}}}{\dot{n}_{\mathrm{CO_2,in}}} \times 100\ \% \tag{8}$$

The gas-side overall mass transfer coefficient was calculated as

$$K_G = \frac{N}{\Delta C_{\mathrm{m}}} \tag{9}$$

Where ΔC_m is the logarithmic mean driving force based on the gas-phase concentrations:

$$\Delta C_{\mathrm{m}} = \frac{\left(C_{\mathrm{g,in}} - C^*_{\mathrm{g,in}}\right) - \left(C_{\mathrm{g,out}} - C^*_{\mathrm{g,out}}\right)}{\ln\left[\left(C_{\mathrm{g,in}} - C^*_{\mathrm{g,in}}\right)\left(\left(C_{\mathrm{g,out}} - C^*_{\mathrm{g,out}}\right)\right)\right]} \tag{10}$$

Here, $C_{g,in}$ and $C_{g,out}$ out are the measured CO_2 concentrations in the inlet and outlet gas and $C^*_{g,in}$ and $C^*_{g,out}$ are the inlet and outlet gas-phase CO_2 concentrations in equilibrium with the corresponding liquid-phase concentrations. The solubility data of Portugal et al. [45] for CO_2 in 1 M potassium glycinate were utilized to calculate the equilibrium concentrations. The gas-phase concentration was plotted against the liquid-phase concentration in the CO_2 partial pressure range relevant to the present experiments (100-1000 kPa), and an exponential curve was fitted to the data (R^2 equal to 97.8%). As a result, the following correlation was found:

$$C^*_{\mathrm{g}} = 1.4 \times 10^{-4} e^{0.014 C_{\mathrm{L}}} \tag{11}$$

Where C_{L} is the liquid-phase CO_2 concentration.

The desorption efficiency was calculated from the measured CO_2 loading in the rich and lean absorbent:

$$\eta_{\mathrm{des}} = \frac{\alpha_{\mathrm{rich}} - \alpha_{\mathrm{lean}}}{\alpha_{\mathrm{rich}}} \times 100\ \% \tag{12}$$

Where η_{des} is the desorption efficiency, α_{rich} and α_{lean} are the CO_2 loadings of the rich absorbent leaving the membrane module and the lean absorbent leaving the stripper, respectively.

2.4.1. Evaluation of individual mass transfer coefficients

The individual mass transfer coefficients can be predicted by various experimental correlations based on the hydrodynamics and configuration of the membrane contactor [12]. For laminar (Re < 2100) flow of liquid inside the hollow fiber, the liquid mass transfer coefficient can be estimated from [47, 48]

$$Sh = \sqrt[3]{3.67^3 + 1.62^3 Gz} \tag{13}$$

Where Sh is the Sherwood number and Gz is the Graetz number, described by

$$Sh = \frac{k_{\mathrm{L}} d_{\mathrm{i}}}{D_{\mathrm{CO_2,L}}} \tag{14}$$

$$Gz = \frac{v_{\mathrm{L}} {d_{\mathrm{i}}}^2}{D_{\mathrm{CO_2,L}} l} \tag{15}$$

Where d_i is the inner diameter of the hollow fiber, $D_{CO_2,L}$ is the diffusivity of CO_2 in the absorbent solution, v_L is the liquid superficial velocity inside the fiber, and l is the membrane fiber length.

For parallel flow of gas in a randomly packed module, the gas mass transfer coefficient can be estimated by the following correlation [49, 50]

$$Sh = \frac{k_{\mathrm{G}} d_{\mathrm{h}}}{D_{\mathrm{CO_2,G}}} = 1.25 \left(\frac{Re\, d_{\mathrm{h}}}{l}\right)^{0.93} Sc^{0.33} \tag{16}$$

Where Re is the Reynolds number, d_{h} is the shell-side hydraulic diameter (Eq. 18), $D_{\mathrm{CO_2,G}}$ is the diffusivity of CO_2 in the feed gas, and Sc is the Schmidt number (Eq. 19):

$$d_h = \frac{{d_{c,i}}^2 - n{d_o}^2}{d_{c,i} + n d_o} \tag{17}$$

Here, $d_{\mathrm{c,i}}$ is the inner diameter of the membrane contactor (shell), d_{o} is the outer diameter of the membrane fiber, and n is the number of fibers. The Reynolds number can be calculated as

$$Re = \frac{4\dot{V}_{\mathrm{G}}}{n d_{\mathrm{o}} \nu_{\mathrm{G}}} \tag{18}$$

Where $\dot{V}_{\mathrm{G}}$ is the gas volumetric flow rate and ν_{G} is the gas kinematic viscosity ($m^2\ s^{-1}$). The Schmidt number is defined by

$$Sc = \frac{\nu_{\mathrm{G}}}{D_{\mathrm{CO_2,G}}} \tag{19}$$

The value of the membrane mass transfer coefficient was estimated by calculation from Eq. 1, with the liquid and gas mass transfer coefficients calculated by the correlations presented above, and the overall mass transfer coefficient set equal to the experimentally found values (Eq. 9). A constant value of the membrane mass transfer coefficient was assumed, with the average value over the liquid flow rate data points taken as the estimate. For comparison, a theoretical estimate for the membrane mass transfer coefficient assuming completely non-wetted operation, was calculating using the following equation [51]:

$$k_M = \frac{\varepsilon D_{\mathrm{CO_2,M}}}{\tau \delta} \tag{20}$$

Where ε is the membrane porosity, $D_{\mathrm{CO_2,M}}$ is the effective diffusivity of CO_2 in the membrane, τ is the membrane tortuosity, and δ is the membrane thickness. The value of the enhancement factor can be estimated based on the calculation of the Hatta number and the infinite enhancement factor [20, 41, 52]. The Hatta number describes the ratio of reaction kinetics to the mass transfer flux at the gas-liquid interface:

$$Ha = \frac{\sqrt{D_{\mathrm{CO_2,L}} k_1 C_{\mathrm{PG,L}}}}{k_{\mathrm{L}}} \tag{21}$$

Where Ha is the Hatta number, k_1 is the forward reaction rate constant for chemical absorption (Eq. 6), and $C_{\mathrm{PG,L}}$ is the concentration of potassium glycinate in the solution. The infinite enhancement factor corresponds to the situation where diffusion of the absorbent in the liquid phase is rate-limiting:

$$E_\infty = \left(\frac{D_{\mathrm{CO_2,L}}}{D_{\mathrm{PG,L}}}\right)^{1/3} + \frac{C_{\mathrm{PG,L}}}{2C_{\mathrm{CO_2,LM}}}\left(\frac{D_{\mathrm{CO_2,L}}}{D_{\mathrm{PG,L}}}\right)^{-2/3} \tag{22}$$

Where $C_{\mathrm{CO_2,LM}}$ is the CO_2 concentration at the liquid-membrane interface and $D_{\mathrm{PG,L}}$ is the diffusivity of potassium glycinate in the solution. The value of the enhancement factor can then be estimated by the DeCoursey solution [53]:

$$E = \frac{-(Ha)^2}{2(E_\infty - 1)} + \sqrt{\frac{(Ha)^4}{4(E_\infty - 1)^2} + \frac{E_\infty (Ha)^2}{(E_\infty - 1)} + 1} \tag{23}$$

Table II presents the values for the parameters used in the calculations.

Table II Parameter values used in the estimation of individual mass transfer coefficients. The values are valid at a temperature of 20 °C, at which the values of the mass transfer coefficients were estimated.

1 M potassium glycinate [21]	
Density, kg m^{-3}	1056.6
Viscosity, kg m^{-1} s^{-1}	1.26×10^{-3}
CO_2 diffusivity, m^2 s^{-1}	1.42×10^{-9}
CO_2 dimensionless Henry's constant	0.73
PG diffusivity, m^2 s^{-1}	3.89×10^{-10}
Forward reaction rate constant k_1, m^3 mol^{-1} s^{-1}	49.68 [23]

Membrane module	
Membrane outer surface area, m^2	1.4
Fiber length, mm	160
Fiber outer diameter, µm	300
Fiber inner diameter, µm	220
Number of fibers	10200
Shell diameter, mm	67
Porosity, -	0.4 [54]
Tortuosity, -	2.5 [50]
Thickness, m	4.0×10^{-5} [54]
Effective CO_2 diffusivity, m^2 s^{-1}	3.87×10^{-6} [54]

Feed gas	
CO_2 diffusivity, m^2 s^{-1} (in air)	1.60×10^{-5} [55]

3. Results and discussion

The main experimental results comprise of the mass transfer performance, as measured by the capture efficiency, CO_2 flux and overall mass transfer coefficient, and the specific energy consumption. In this section, the effect of the main varied operating parameters on the steady-state absorption and desorption performance is discussed. Section 3.1 presents results from the experiments without vacuum employed in the solvent regeneration, with the primary aim of assessing the absorption performance of the membrane contactor. Section 3.2 presents a more comprehensive set of results from the vacuum solvent regeneration for assessment of the CO_2 desorption efficiency and the resulting mass transfer performance of the membrane contactor. Section 3.3 presents the calculated individual mass transfer coefficients. Finally, Section 3.4 presents data from a 6-day stability test which was performed to assess the long-term stability and performance of the unit.

3.1. Non-vacuum desorption

Figure 2 presents the effect of the liquid flow rate on the CO_2 capture efficiency and the overall mass transfer coefficient. Desorption was carried out at 80 °C. The liquid flow rate was varied from 0.75 l/min (velocity 0.03 m/s) to 1.5 l/min (velocity 0.06 m/s). The capture efficiency was found to increase from 54 % at the flow rate of 0.75 l/min to 72 % at 1.5 l/min, with the corresponding overall mass transfer coefficients ranging from $4.7 \cdot 10^{-5}$ m s^{-1} to $7.9 \cdot 10^{-5}$ m s^{-1}. The observed trend is similar to previous studies with potassium glycinate absorbent [24, 25]. The mass transfer coefficients are also similar in magnitude to those reported by Lu et al. [25] for a similar membrane absorption system. With increasing liquid velocity, the liquid-side mass transfer resistance is decreased due to decreased thickness of the boundary layer [42], increasing the overall mass transfer rate.

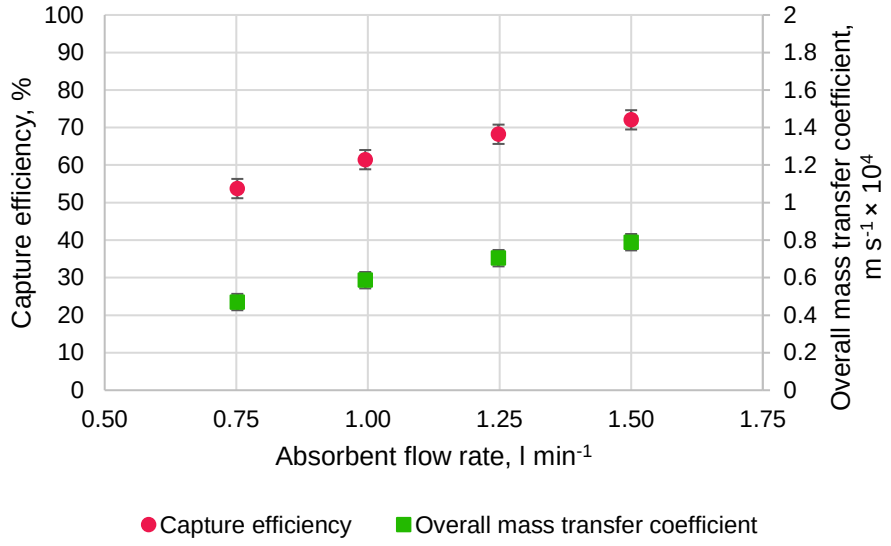

Figure 2 Effect of absorbent flow rate on the CO_2 capture efficiency and the overall mass transfer coefficient. Absorbent 1 M potassium glycinate, absorption temperature 20 °C, regeneration temperature 80 °C, feed gas 10 % CO_2 (balance N_2), gas flow rate 5.0 l min^{-1}.

With sufficiently high flow rates and low CO_2 loadings over the membrane length, there is an excess in free amino acid salt present at the liquid interface, and the absorption is controlled by the kinetics of chemical reaction [20, 46]. In this fast reaction regime, the CO_2 flux and overall mass transfer coefficient are not significantly increased with increasing liquid flow rate. At lower liquid flow rates and/or higher loadings, the free amino acid salt at the liquid interface is depleted, and the absorption is controlled by the diffusion of the reacting species. Here, a roughly linear increase can be found in the overall mass transfer coefficient with increasing liquid flow rate. Based on the relatively low liquid velocities combined with high lean CO_2 loadings of the absorbent solution (ranging from 0.49 at the flow rate of 0.75 l min^{-1} to 0.51 at 1.5 l min^{-1}), some degree of amino acid salt depletion could be expected [20] under the present conditions. The high

lean loadings are caused by the ineffective desorption without utilization of vacuum in the stripper, as discussed below.

Figure 3 presents the effect of the absorption temperature on the CO_2 capture efficiency and the overall mass transfer coefficient calculated from experimental data using Eqs. (8) and (9). The capture efficiency was found to decrease from 70 % to 56 % with the temperature increased from 10 °C to 30 °C. The mass transfer coefficient correspondingly decreased from $7.4 \cdot 10^{-5}$ m s^{-1} to $5.0 \cdot 10^{-5}$ m s^{-1}. An opposite effect is usually found with amine absorbents [56]. However, Yan et al. [24] also found a decreasing absorption rate with increasing temperature using potassium glycinate. In contrast, Lu et al. [25] found that increasing the temperature from 20 °C to 40 °C resulted in an increased overall mass transfer coefficient with the same solvent.

Generally, increased mass transfer at higher temperatures would be expected both due to the increased rate of chemical reaction and increased diffusivity of CO_2 in the liquid. Thus, the observed decrease is likely due to reduced CO_2 solubility at higher temperature [45]. Under the present conditions, the CO_2 loading in the liquid is high, resulting in a high equilibrium concentration in the gas-phase (following Eq. 11). The lean loading values at the absorption temperatures of 10, 20 and 30 °C were measured at 0.52, 0.50, and 0.52 mol mol^{-1}, respectively. There is no trend observed and the lower value at 20 °C can likely be explained by experimental error. The loadings at all temperatures are essentially the same but the equilibrium loading (corresponding to the CO_2 partial pressure in the membrane module) is decreased with increasing temperature. As a result, the mass transfer driving force is decreased, offsetting the favorable effects of increased temperature on the mass transfer rate.

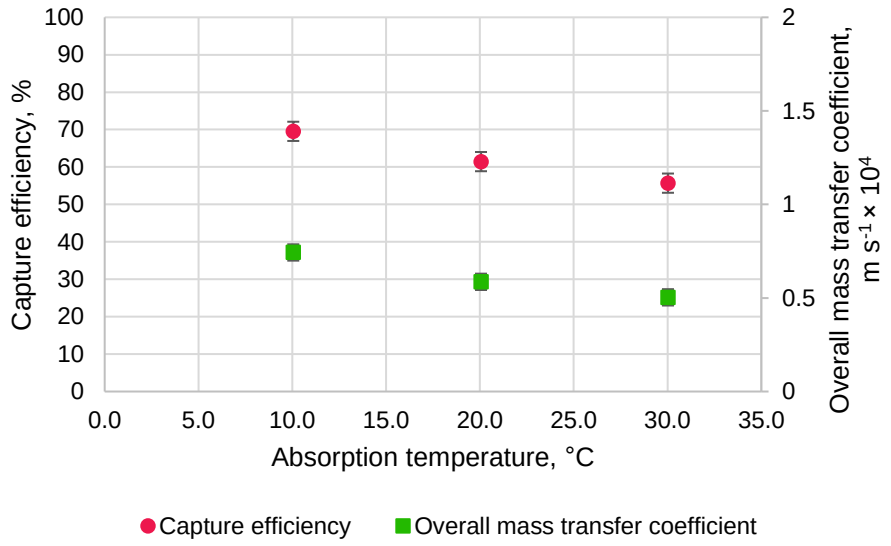

Figure 3 Effect of absorption temperature on the CO_2 capture efficiency and the overall mass transfer coefficient. Absorbent 1 M potassium glycinate, liquid flow rate 1.0 l min^{-1}, regeneration temperature 80 °C, feed gas 10 % CO_2 (balance N_2), gas flow rate 5.0 l min^{-1}.

Figure 4 shows the effect of the feed gas CO_2 concentration on the CO_2 capture efficiency and the overall mass transfer coefficient. The capture efficiency decreased from 66 % to 56 % with the increasing feed concentration. At otherwise identical conditions, the higher CO_2 concentration in the feed resulted in a larger fraction of CO_2 exiting the module uncaptured, as is expected.

Increasing the feed CO_2 concentration should result in an increased absorption rate due to the increasing mass transfer driving force and increased rate of chemical absorption. This was observed also here, as the CO_2 flux (not shown) was increased with the increasing CO_2 concentration. However, the value of the mass transfer coefficient decreased from $6.8 \cdot 10^{-5}$ m s^{-1} to $4.8 \cdot 10^{-5}$ m s^{-1} with the feed concentration increased from 5 vol-% to 15 vol-%. The decreasing mass transfer coefficient is most likely caused by changes in the rate of chemical absorption. Again, with high CO_2 loadings (approximately 0.5), the concentration of free amine in the absorbent is relatively low, and depletion at the reactive interface may have taken place. Possibly, this depletion was more significant as the CO_2 concentration was increased and the reaction rate correspondingly increased. This would result in a lower value of the enhancement factor, and thus a lower value of the overall mass transfer coefficient, as described by Eq. 1.

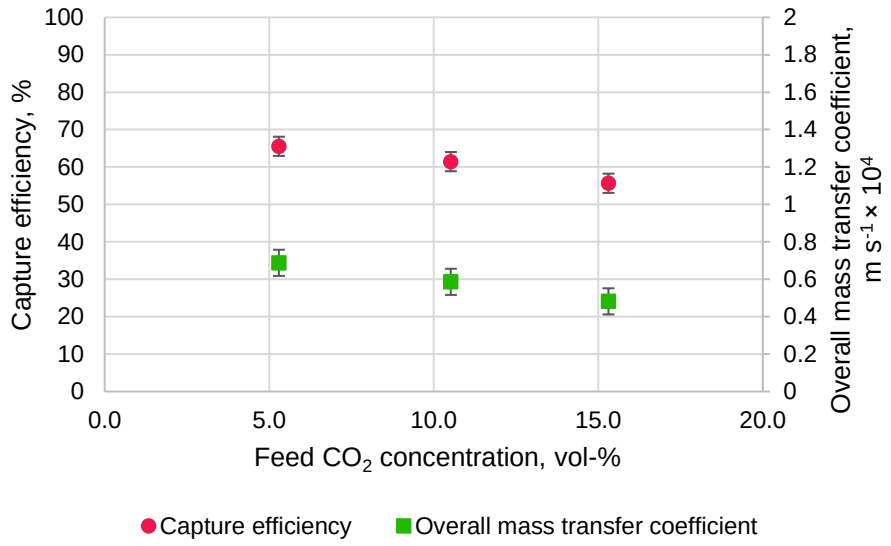

Figure 4 Effect of feed gas CO_2 concentration (balance N_2) on the CO_2 capture efficiency and the overall mass transfer coefficient. Absorbent 1 M potassium glycinate, liquid flow rate 1.0 l min^{-1}, absorption temperature 20 °C, regeneration temperature 80 °C, gas flow rate 5.0 l min^{-1}.

Figure 5 presents the variation in CO_2 capture efficiency and the overall mass transfer coefficient with the solvent regeneration temperature varied from 60 °C to 80 °C. The capture efficiency was found to range from only 10 % at the regeneration temperature of 60 °C to 61 % at 80 °C. The corresponding overall mass transfer coefficients ranged from $0.7 \cdot 10^{-5}$ m s^{-1} to $4.9 \cdot 10^{-5}$ m s^{-1}. At relatively low regeneration temperatures, and with no vacuum employed, the steady-state CO_2 absorption rate is strongly limited by the efficiency of CO_2 desorption from the solution, especially at regeneration temperatures below 80 °C. Increasing the temperature results in a significant increase in the desorption rate due to the lower equilibrium loading [45] as dictated by the chemical equilibrium (Eq. 3-5) and the increased rate of the reverse reactions leading to release of CO_2 from solution. In addition, mass transfer rate of CO_2 from the solution to the gas phase in the stripper increases as a result of higher CO_2 diffusivity and lower solution viscosity at higher temperature [43].

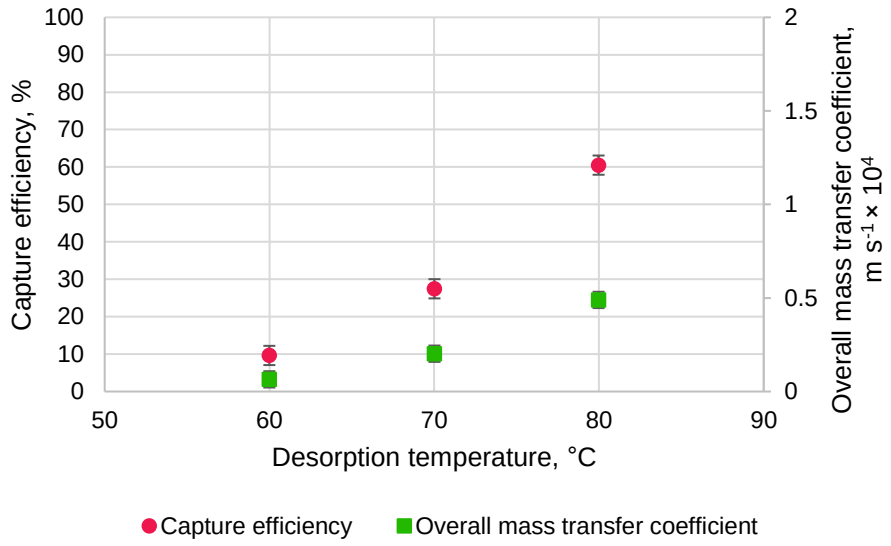

Figure 5 Effect of regeneration temperature on CO_2 capture efficiency and the overall mass transfer coefficient. Absorbent 1 M potassium glycinate, liquid flow rate 1.0 l min^{-1}, absorption temperature 20 °C, feed gas 10 % CO_2 (balance N_2), gas flow rate 5.0 l min^{-1}.

Regardless of the desorption temperature, the absorption rate is limited by the high CO_2-loading in the lean absorbent, which ranges from 0.55 mol mol^{-1} at 60 °C to 0.50 mol mol^{-1} at 80 °C. He et al. showed that the CO_2 absorption rate of amino acid salt solutions is strongly dependent on the CO_2 loading [57]. With various amino acid salts including potassium glycinate, the absorption rate was found to decrease by more than 80 % with the loading changing from zero to 0.4 mol mol^{-1}. The effect of the CO_2 loading on the absorption rate could be explained by the influence of both physical and chemical absorption. The higher loading results in a decreased driving force for mass transfer through the membrane from the gas to the liquid phase. At the same time, according to Eq. 6, the rate of chemical absorption is decreased due to the lowered concentrations of free amino acid at the membrane-liquid interface, which results in a lower value for the enhancement factor and lower overall absorption rate.

3.2. Vacuum desorption

The main objective of the non-vacuum results discussed above was to characterize the membrane mass transfer performance, as measured by the overall mass transfer coefficient, with variation of key operating parameters. In the vacuum desorption experiments described in this section, the focus is shifted on to the performance of the whole unit consisting of the absorption and desorption stages. The key issue here is the effect of the desorption performance, and the resulting CO_2 loading of the lean absorbent, on the mass transfer performance of the membrane contactor.

3.2.1. Desorption temperature and vacuum pressure

Desorption of CO_2 from the rich solution takes place by shifting the equilibrium of the absorption reactions (Eq. 3-5) to the reverse side, followed by diffusion of the released CO_2 from the bulk liquid to the gas-liquid interface, and finally to the gas phase. The shift in the chemical equilibrium leads to decreasing solubility of CO_2 in the absorbent solution at elevated temperatures. In conventional amine-based CO_2 capture processes, desorption is performed at temperatures above 100 °C to facilitate effective release of CO_2 from solution [4]. However, operating at lower desorption temperatures would be preferable to minimize heat energy consumption, to allow utilization of low-grade heat, and to avoid solvent losses and environmental concerns related to degradation of the absorbent.

To decrease the desorption temperature, vacuum was employed in the experiments described here. By utilizing vacuum, the partial pressure of CO_2 in the gas phase can be reduced, leading to decreased CO_2 solubility in the liquid and increased driving force for the transfer of CO_2 from the liquid phase. In addition, the vacuum pump continuously removes the released CO_2 from the desorption vessel, providing a sweeping effect which is conventionally achieved by evaporating water from the solution. Minimizing the evaporation of water while maintaining a high CO_2 desorption flux would minimize the energy input required for regeneration of the solvent [36].

Figure 6 presents the CO_2 capture efficiency and the overall mass transfer coefficient at the membrane contactor with the desorption temperature varied at 60-80 °C and vacuum pressure at 300-800 mbar. The maximum temperature of 80 °C was dictated by the operating limits of the experimental unit, while the low limit of the vacuum pressure was set by the water vapor pressure at each temperature. Clearly, the absorption performance is favored both by higher temperature and lower pressure at desorption. At 60 °C, lowering the pressure from 800 mbar to 300 mbar results in a 4.7-fold increase in the value of the overall mass transfer coefficient. As another example, at the vacuum pressure of 500 mbar the overall mass transfer coefficient at 80 °C is higher by a factor of 7.4 compared to that at 60 °C. Correspondingly, the capture efficiency is significantly increased at higher temperature and lower vacuum pressure, with efficiency above 90 % reached at 80 °C and 500-600 mbar.

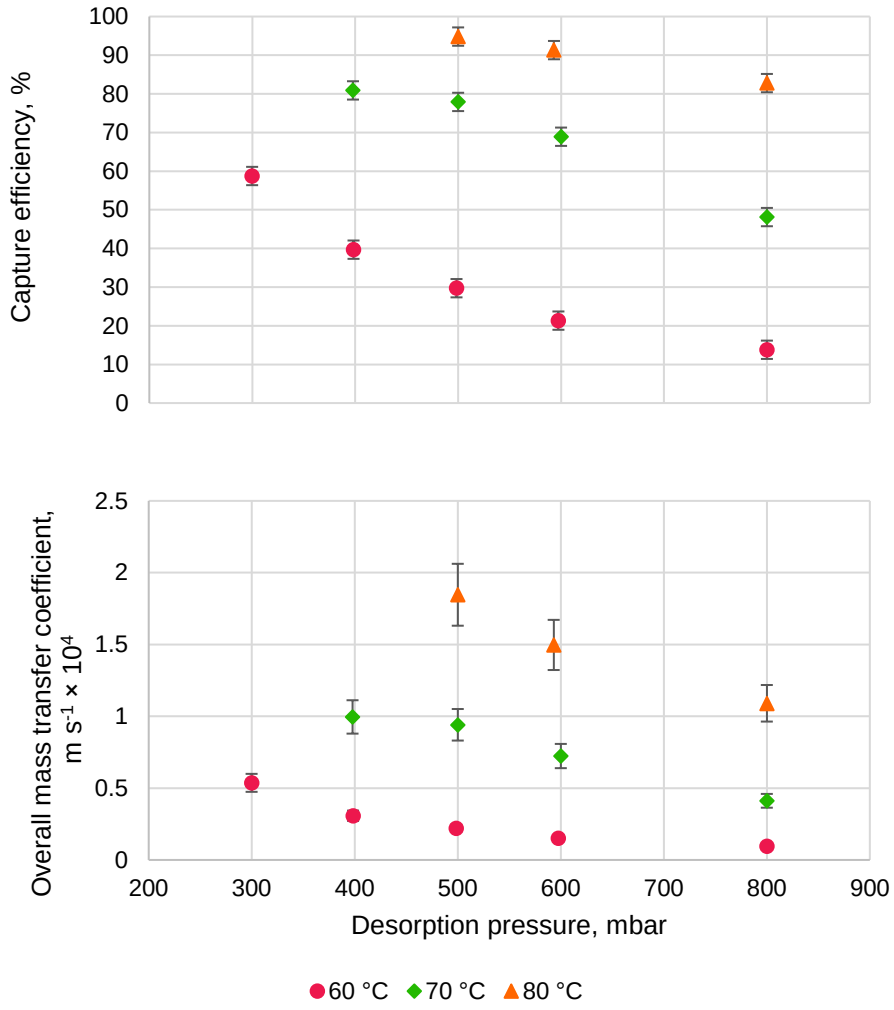

Figure 6 CO_2 capture efficiency and absorption overall mass transfer coefficient with the temperature and vacuum pressure varied in solvent regeneration. Absorbent 1 M potassium glycinate, liquid flow rate 1.0 l min^{-1}, absorption temperature 20 °C, feed gas 10 % CO_2 (balance N_2), gas flow rate 5.0 l min^{-1}. The 95% confidence interval of the overall mass transfer coefficient was determined at the temperature of 80 °C. At the lower temperatures, a similar relative deviation is assumed. All measurements at vacuum pressures 500-800 mbar were previously presented as the corresponding CO_2 fluxes in a previous publication [40].

The improved absorption performance at more favorable desorption conditions is explained by changes in the lean loading, as depicted in Figure 7. With more efficient desorption of CO_2 from the solution at increased temperature and reduced pressure, the lean liquid entering the membrane contactor is able to absorb CO_2 at higher rate. At 60 °C, the measured lean loading was reduced from 0.57 mol mol^{-1} to 0.48 mol mol^{-1} with the vacuum pressure lowered from 800 to 300 mbar. At 80 °C, the loading varied from 0.48 mol mol^{-1} at 800 mbar to 0.42 mol mol^{-1} at 500 mbar. However, even at the optimal conditions of 80 °C and

500 mbar, the desorption efficiency remained low, at 5.5 ± 1.42 %. This also resulted in a cyclic CO_2 capacity (the difference between rich and lean solvent loading) of only 0.02 ± 0.006 mol. In benchmark amine capture processes, the cyclic capacity is above 0.2 mol [15]. As such, the overall CO_2 capture rate here remains strongly limited by the desorption performance.

To improve the performance, lower vacuum pressures and/or higher temperatures should be tested, and the configuration of the desorption unit improved. The latter could be achieved e.g. by introducing packings to the desorption vessel, installing a reboiler, or by replacing the vessel with alternative equipment such as a membrane contactor [38].

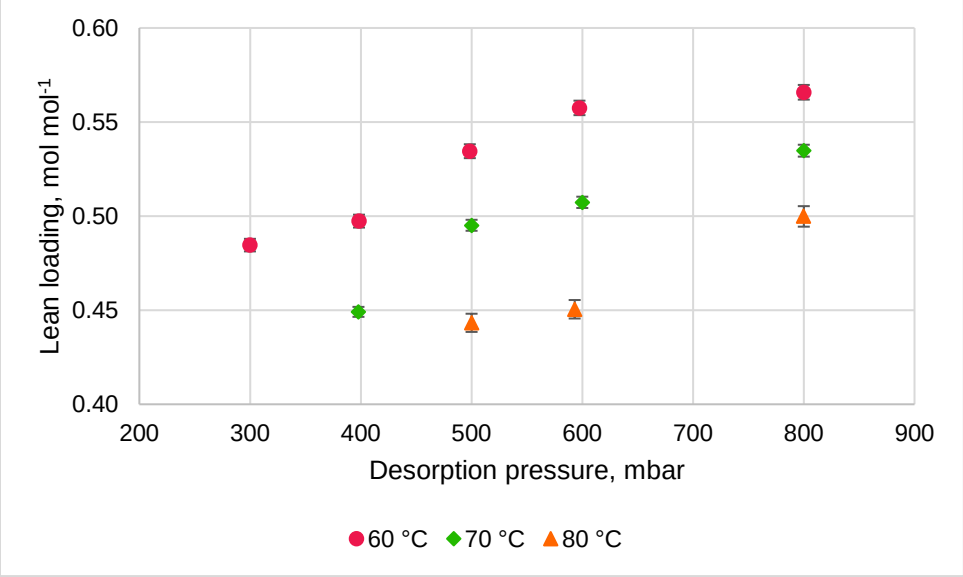

Figure 7 CO_2 loading of the lean absorbent solution with the temperature and vacuum pressure varied in solvent regeneration. Absorbent 1 M potassium glycinate, liquid flow rate 1.0 l min^{-1}, absorption temperature 20 °C, feed gas 10 % CO_2 (balance N_2), gas flow rate 5.0 l min^{-1}. Error bars represent the standard deviation from three repeated titrimetric analyses. All measurements at vacuum pressures 500-800 mbar were previously reported as the corresponding CO_2 fluxes in a previous publication [40].

The limiting effect of the desorption performance and the resulting high lean CO_2 loading was studied by collecting data from a start-up period during which a fresh, unloaded absorbent was circulated and the CO_2 loading was continuously increased during CO_2 absorption. By collecting a series of liquid samples during the start-up, the variation of the absorption rate with the lean loading could be followed, with results shown in Figure 8a. The absorption rate is decreased by approximately 35% with the lean loading increasing from 0.02 mol mol^{-1} to 0.45 mol mol^{-1}. This decrease is consistent with the data from He et al. [57], who measured the CO_2 absorption rates in a membrane contactor at various CO_2 loadings and temperatures using potassium glycinate and other amino acid salt absorbents.

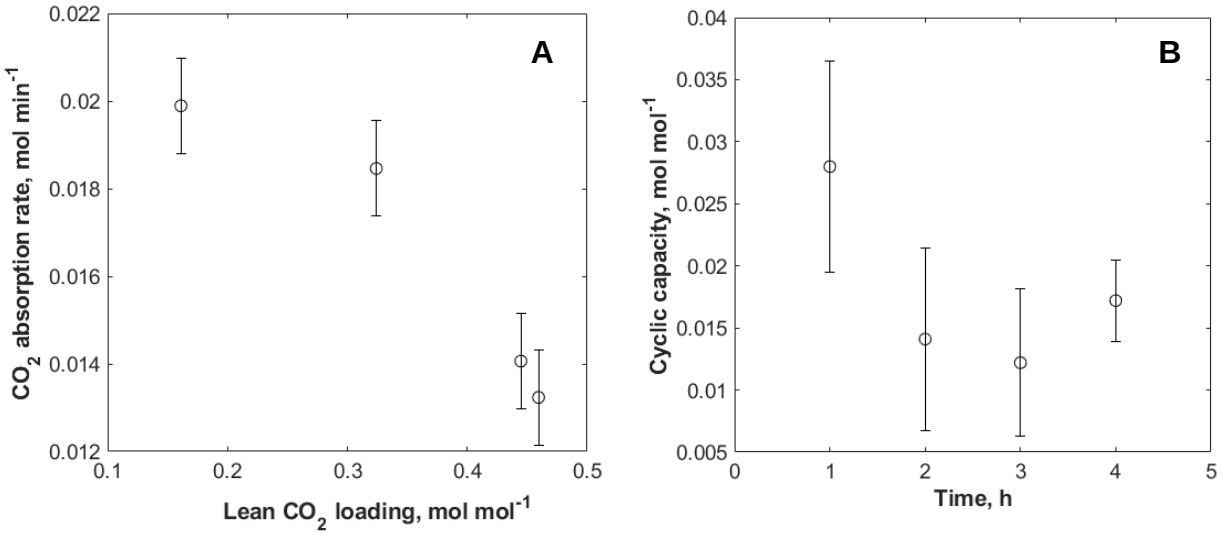

Figure 8 A) Variation of CO_2 absorption rate with the lean solvent CO_2 loading and B) variation of cyclic CO_2 capacity during a start-up period of five hours. Absorbent 1 M potassium glycinate, liquid flow rate 1 l min^{-1}. Absorption temperature 20 °C, regeneration temperature 70 °C and pressure 500 mbar. Feed gas 10 % CO_2 (balance air), gas flow rate 5.0 l min^{-1}.

The lean loadings depicted in Figure 8a are based on lean solvent samples collected once per hour, with the first sample collected one hour after initiating CO_2 absorption. Rich solvent samples were collected simultaneously to the lean samples. Based on the difference in lean and rich loadings, the cyclic capacity at the sampling points was determined, with results shown in Figure 8b. Following one hour of absorption, a higher cyclic capacity (0.028 mol mol^{-1}) is found compared to the later data points where the cyclic capacity values are in a similar range (0.012-0.017 mol mol^{-1}) to those found during steady-state experiments. Accordingly, the desorption efficiency is much higher (14.8 %) at the initial data point compared to 2.7 % to 4.2 % at the later points.

Generally, desorption is expected to be more effective at higher solvent CO_2 loading due to increased driving force. The higher efficiency found after one hour of operation is likely explained by changes in the gas atmosphere present in the desorption vessel. Prior to starting the operation and initiating the absorption/desorption cycle, the vessel is filled with air and the partial pressure of CO_2 is very low. As more CO_2 is absorbed into the circulating solution and then released in the desorption vessel, the partial pressure of CO_2 is gradually increased. This explanation is supported by CO_2 concentration measured at the outlet gas from the desorption vessel. After one hour, the CO_2 concentration is nearly 0 % but the concentration gradually increases, reaching the final steady-state value of almost 90 % after 3.5 hours of operation. This

finding also suggests that the CO_2 partial pressure in the desorption vessel may be a limiting factor for the desorption performance in the current setup.

3.2.2. Liquid flow rate

Figure 9 presents the effect of the liquid flow rate on the CO_2 flux and the overall mass transfer coefficient with desorption performed under 600 mbar vacuum. The CO_2 fluxes found here are in the order of 50 % lower compared to the values from Yan et al. [24] at similar liquid velocities. This difference can be explained by the higher CO_2 feed concentration in that study (14 %) and more importantly, the use of unloaded potassium glycinate absorbent, compared to the circulated, CO_2-loaded solvent used here. The effect of the flow rate on the CO_2 flux is not very significant, with the flux ranging from 2.3×10^{-4} mol m^{-2} s^{-1} at 0.75 l min^{-1} to 2.6×10^{-4} mol m^{-2} s^{-1} at 1.5 l min^{-1}. The liquid-side physical mass transfer coefficient generally increases at increasing liquid velocity, which should increase the absorption rate. This implies that under these conditions, significant depletion of free amine at the interface does not take place, and absorption takes place in a regime significantly controlled by reaction kinetics [20].

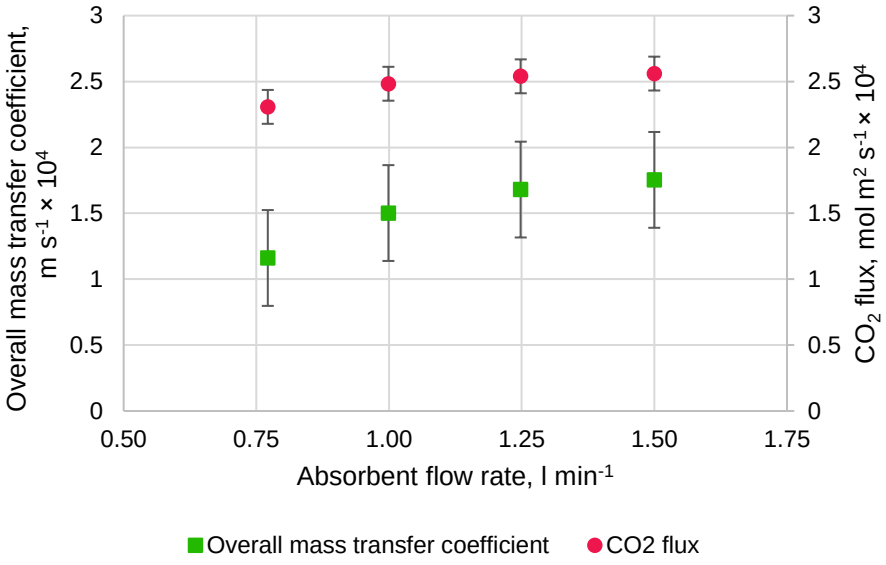

Figure 9 Effect of absorbent flow rate on the overall mass transfer coefficient and the CO_2 flux. Absorbent 1 M potassium glycinate, absorption temperature 20 °C, regeneration temperature 80 °C and pressure 600 mbar, feed gas 10 % CO_2 (balance N_2), gas flow rate 5.0 l min^{-1}.

A slightly more significant change is observed in the values of the overall mass transfer coefficient, ranging from 1.2×10^{-4} m s^{-1} at 0.75 l min^{-1} to 1.8×10^{-4} m s^{-1} at 1.5 l min^{-1}. The magnitude of these values is consistent with those presented by Lu et al. [25] for potassium glycinate absorbent used in a PP membrane

contactor. The increase in the overall mass transfer coefficient is primarily due to the decreasing liquid-side mass transfer resistance with increasing liquid velocity. The calculated values of the overall mass transfer coefficient are also affected by the solvent CO_2-loading due to the variation in the logarithmic mean driving force (Eq. 10). As such, the values of the overall mass transfer coefficient are sensitive to the equilibrium relationship used in the calculation of the gas-side equilibrium CO_2 concentrations.

The variation in the CO_2-loading of the lean and rich absorbent with the liquid flow rate is presented in Figure 10. The lean loading decreases with increasing liquid flow rate. However, as is evident from the CO_2 fluxes in Figure 9, the decreased CO_2-loading in the absorbent entering the membrane module does not have a significant impact on the CO_2 absorption rate. Such an impact would be expected based on the higher physical mass transfer driving force (i.e. lower gas-side equilibrium concentration), and the increased availability of free amine for reaction. This again points to the significance of the intrinsic chemical reaction rate (as measured by the kinetic constant k_1 in Eq. 6) as a significant limiting factor for the absorption rate under the present conditions.

As the increase in the absorption rate is not very significant, the relative increase in the CO_2-loading over the membrane module is decreased at increasing liquid flow rate, as the residence time is correspondingly decreased. This is observed from the differences between the rich and lean loadings in Figure 10. The relative differences range from 5 % at 0.75 l min^{-1} to 3 % at 1.5 l min^{-1}. In absolute terms, the amount of CO_2 accumulated in the absorbent over the module is decreased from 0.024 mol to 0.013 mol, respectively. From the discussion above, it appears that the absorbent is more effectively utilized at the lower range of the flow rates studied, and the higher flow rates would result in unnecessary increases in operating costs from circulation and heating of the solvent.

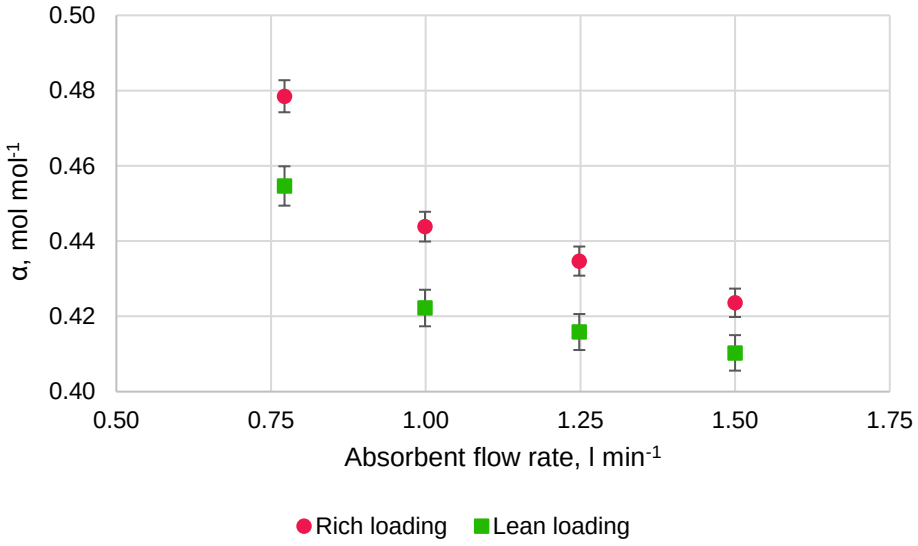

Figure 10 CO_2 loading of the rich and lean absorbent with absorbent flow rate varied. Absorbent 1 M potassium glycinate, absorption temperature 20 °C, regeneration temperature 80 °C and pressure 600 mbar, feed gas 10 % CO_2 (balance N_2), gas flow rate 5.0 l min^{-1}.

3.2.3. CO_2 concentration

Figure 11 presents the variation in CO_2 flux and overall mass transfer coefficient with the feed CO_2 concentration varied from 5 to 15 vol-%. A linear increase in the CO_2 flux was found with the increasing feed concentration as a result of the increased driving force for mass transfer and chemical absorption. At the same time, a slightly decreasing overall mass transfer was found with the increasing feed concentration. The change in the overall mass transfer coefficient could be a result of decreasing amino acid concentration at the reaction interface, resulting in decreasing enhancement factor and higher overall mass transfer resistance. Due to these limitations, the increasing mass transfer driving force is not completely utilized. The corresponding capture efficiencies (not shown) range from 94.6 % at 5 % CO_2 feed to 90.2 % at 15 % CO_2 feed, showing that the efficiency can be maintained at a high level over a wide range of feed concentrations under the present conditions.

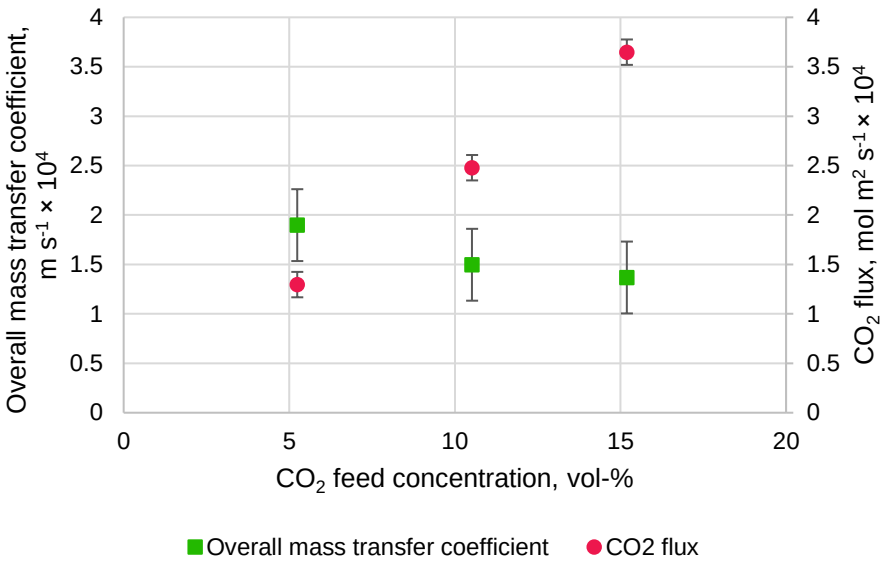

Figure 11 Effect of feed CO_2 concentration (balance N_2) on the overall mass transfer coefficient and the CO_2 flux. Absorbent 1 M potassium glycinate, liquid flow rate 1.0 l min^{-1}, absorption temperature 20 °C, regeneration temperature 80 °C and pressure 600 mbar, gas flow rate 5.0 l min^{-1}.

3.3. Individual mass transfer coefficients in absorption

The magnitude of the individual mass transfer coefficients with the liquid flow rate varied was evaluated based on the procedure described in Section 2.4.1. The values of the corresponding individual mass transfer coefficients are presented in Table III, together with the values of the Reynolds number and enhancement factor. The liquid-side resistance constitutes the major fraction (88-89%) of the overall mass transfer resistance, while the membrane resistance is also significant (11-12%). The gas-side resistance is negligible. The differences in the enhancement factor are due to variation in the lean absorbent loading (Figure 10) and small deviations in the feed gas CO_2 partial pressure.

Table III Values of the Reynolds number, enhancement factor, and individual mass transfer coefficients with the liquid velocity varied. Absorbent 1 M potassium glycinate, absorption temperature 20 °C, regeneration temperature 80 °C and pressure 600 mbar , feed gas 10 % CO_2 (balance N_2), gas flow rate 5.0 l min^{-1}.

Liquid velocity, m s^{-1}	Re, -	E, -	$k_L \times 10^5$, m s^{-1}	$k_G \times 10^3$, m s^{-1}	$k_m \times 10^4$, m s^{-1} (calculated from experiments)	$k_m \times 10^2$, m s^{-1} (theoretical)
0.033	6.1	12.9	2.78	1.14	2.92 ± 0.40	1.55
0.043	7.9	24.9	2.87			
0.054	9.9	22.3	2.98			
0.064	11.9	26.2	3.07			

Compared to the data from Feron and Jansen [22] for a transversal-flow PP membrane module and proprietary amino-acid salt absorbent, both the liquid and membrane mass transfer coefficients are almost two orders of magnitude lower here. The difference in the liquid mass transfer coefficient could be explained by the different flow configuration, but the difference in the membrane mass transfer coefficient is significant and cannot be explained by differences in the membrane properties. Both the liquid and membrane mass transfer coefficients are of the same order of magnitude to the values reported by Franco et al. [58] for PP module and MEA absorbent (7.8×10^{-4} m s^{-1} and 7.0×10^{-4} m s^{-1} for liquid and membrane, respectively). Compared to these values, the membrane mass transfer coefficient is 67% lower in our case. The membrane resistance here is comparable to other studies with PP membranes and amine absorbents [59, 60, 61].

As PP membranes are commonly partially wetted by MEA, a lower membrane resistance (higher mass transfer coefficient) would be expected with potassium glycinate as the wetting tendency is lower. Even a minor degree of membrane wetting results in a sharp increase in the membrane mass transfer resistance [62]. It appears that some degree of degradation in the membrane performance due to wetting or other effects (e.g. fouling) may have taken place in the present work, which is plausible as the same module had been used for an extended period of time prior to the experiments discussed in this section. This possibility is also reflected by the fact that the theoretical membrane mass transfer coefficient, which assumes completely non-wetted operation, is higher than the calculated value by a factor of almost 50. It should be noted that the theoretical value is itself subject to uncertainties in the membrane properties used in the calculation (e.g. the values of porosity and tortuosity). Generally, any uncertainties involved in the mass transfer analysis are likely lumped into the membrane mass transfer coefficient as the single adjusted parameter [63]. A likely source of such uncertainty is the estimation of the enhancement factor at the high liquid CO_2 loadings under present conditions.

3.4. Long-term stability and CO_2 selectivity

To check for potential membrane wetting or other stability issues, a stability test was performed over a period of six days. The test was run at the desorption conditions of 70 °C and 500 mbar, with the system running continuously during the day and shut off for the night. Instead of nitrogen, CO_2 was mixed with air in the feed gas in order to include the potential effects of oxygen on the solvent or membrane stability. The same batch of absorbent liquid was used throughout the test, and the liquid was not drained in-between the runs, maintaining constant contact between the absorbent and the membrane contactor. Water evaporated from the solution in the desorption vessel and condensed in the vacuum pump condenser was replaced to the solution after each day to maintain the liquid volume and concentration.

Figure 12 presents the continuous variation in the CO_2 concentration at the membrane outlet over the testing period. The concentration remains stable over the period, with no decline in performance found. This suggests that no significant membrane wetting took place over a total of approximately 33 hours, which is of course a very limited time period concerning long-term operation. A similar results was found by Yan et al. [24] over 40 hours of operation with potassium glycinate and PP membrane contactor. Here, the membrane module had been used for months of experiments prior to the stability test. It is possible that some performance decline during the initial operating period had taken place, as has been observed in the case of amine absorbents [62]. However, significant changes in the performance over the entire period of use for the membrane module were ruled out by repeated experiments.

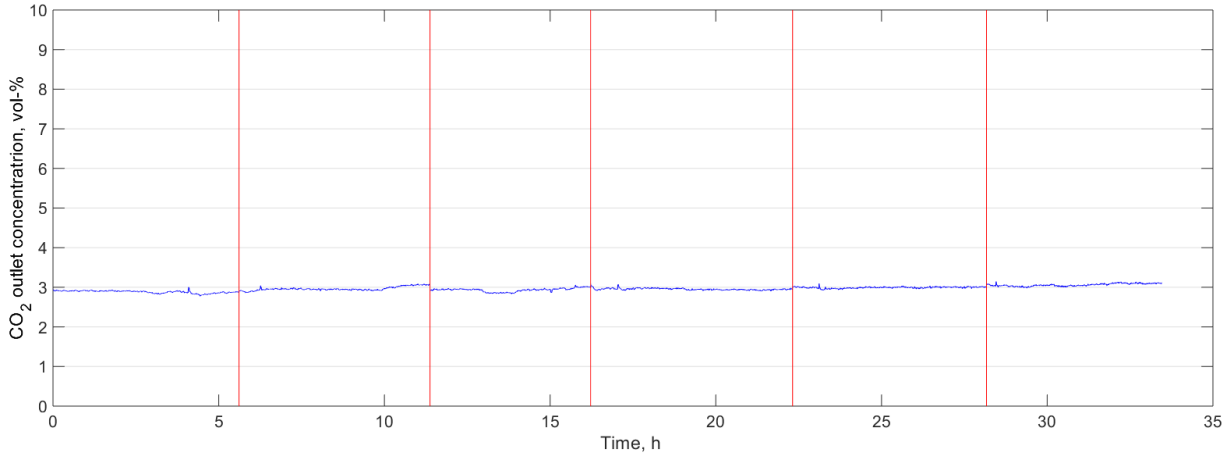

Figure 12 CO_2 concentration of the membrane outlet gas over six days of continuous operation. Absorbent 1 M potassium glycinate, liquid flow rate 1 l min^{-1}. Absorption temperature 20 °C, regeneration temperature 70 °C and pressure 500 mbar. Feed gas: 10 % CO_2, balance air. Gas flow rate 5.0 l min^{-1}.

Based on lean and rich solvent samples collected once per day, the cyclic capacity during the stability test ranged from 0.016 ± 0.007 mol mol^{-1} to 0.037 ± 0.011 mol mol^{-1} with no trend observed during the operating period. Considering the experimental uncertainty, the values seem to be in a similar range to those found

at the later data points collected during start-up (Figure 8b). The start-up data was collected prior to beginning the stability test, using the same batch of solvent and identical operating conditions. This suggest that the cyclic capacity found at the end of the start-up period and subsequent long-term operation correspond the steady-state value at the corresponding operating conditions.

The CO_2 and oxygen concentrations in the product gas leaving the desorption stage were also monitored during the stability test. The CO_2 concentration varied in the range of 84.4 to 89.4 vol-%, and the oxygen concentration in the range of 6.1 to 8.5 vol-%. This implies that co-absorption of oxygen from the feed air takes place despite the high selectivity of the absorbent solution towards CO_2. Also, any oxygen absorbed is expected to desorb effectively under heating and vacuum, resulting in a relatively high cyclic capacity for oxygen. As a result, the apparent CO_2/O_2 selectivity is in the range of only 10.5 to 14.4 during the continuous runs discussed here. It should be noted that minor air leaks in the vacuum system could not be completely ruled out, and the oxygen concentration could be affected by air intrusion. However, the point could be made that in the operation of membrane contactor systems under low cyclic capacity and high lean loading conditions, the absorption of oxygen may not be negligible, as is commonly assumed in modelling approaches [63].

3.5. Summary of results

The effect of key operating parameters on the CO_2 absorption performance of the membrane contactor was assessed. In a series of experiments without vacuum employed, the overall mass transfer coefficient was found to be favored by higher liquid flow rates, higher CO_2 concentration in the feed gas, and interestingly, by lower absorption temperatures. Desorption efficiency was improved by increasing the temperature at the solvent regeneration stage from 60 °C to 80 °C, which resulted in higher CO_2 capture efficiency and higher overall mass transfer coefficient at the absorption stage due to the reduced CO_2 loading in the lean absorbent entering the membrane module.

The introduction of vacuum improved the desorption performance, which in turn resulted in higher capture efficiencies and overall mass transfer coefficients. Both were increased at higher temperatures and lower vacuum pressures in the range of 60-80 °C and 300-800 mbar. The low limit of the vacuum pressure was set by the water boiling point at the corresponding temperature. However, the desorption efficiency was still low due to mass transfer limitations in the stripper with only 5.5 % of the CO_2 released from the amount absorbed in the solution. As a result, the lean CO_2 loading remained as high as 0.42 mol mol^{-1}, limiting the CO_2 absorption rate in the membrane contactor.

With vacuum desorption employed, the CO_2 flux increased with increasing liquid flow rate, but the effect was relatively small. This suggests that absorption took place under a regime significantly controlled by the kinetics of the reactive absorption. A more significant increase with liquid flow rate was found in the overall mass transfer coefficient, as the liquid-side mass transfer resistance was decreased at increasing liquid

velocity. The highest value of the overall mass transfer coefficient reached 1.8×10^{-4} m s^{-1}, which is comparable to values presented in literature for similar systems.

The liquid and gas mass transfer resistances were predicted using correlations available in literature, including estimation of the enhancement factor for chemical absorption. The membrane resistance was estimated based on the experimentally obtained overall mass transfer coefficients and measured absorption data. This value was significantly lower compared to a theoretical estimate assuming non-wetted operation, which suggests possibility of partial wetting of the membrane. The values of the individual mass transfer coefficients are reasonably comparable to literature data on amine and amino acid salt absorbents and PP membrane contactors. The overall mass transfer resistance was found to be dominated by the liquid-side resistance, constituting almost 90 % of the overall resistance.

4. Conclusions

The mass transfer performance of a continuously operated CO_2 capture unit based on a membrane contactor and vacuum solvent regeneration was characterized. The system utilized a polypropylene membrane contactor with aqueous potassium glycinate as absorbent. The present results provide an overview on the effects of key operating parameters on the absorption performance, as measured by the gas-side overall mass transfer coefficient.

In the current experimental set-up, steady-state performance is limited by inefficient desorption resulting in high CO_2 loading in the lean absorbent entering the membrane contactor, decreasing the CO_2 absorption rate. Desorption performance was improved by introduction of vacuum and by increasing the desorption temperature. The highest value of the overall mass transfer coefficient was found with desorption performed at 80 °C and 500 mbar. The overall mass transfer coefficient increased with increasing liquid flow rate. The highest value of the overall mass transfer coefficient was 1.8×10^{-4} m s^{-1}. The individual mass transfer resistances were evaluated, and the overall mass transfer resistance was found to be dominated by the liquid-side resistance at almost 90 % of the total resistance. The membrane mass transfer resistance calculated from experimental data is high compared to a theoretical value which assumes completely non-wetted operation of the membrane contactor, suggesting partial wetting of the membrane under present conditions.

Operation under desorption-limited conditions allows the characterization of the membrane mass transfer performance at high lean CO_2 loadings, as opposed to unloaded absorbent solutions used in the majority of previous studies. Stable performance of the unit and the membrane contactor was also demonstrated during a stability test with over 30 hours of operation.

5. Nomenclature

A	membrane surface area, m^2
C	concentration, mol m^{-3}
C^*	equilibrium concentration, mol m^{-3}
D	diffusivity, m^2 s^{-1}
d	diameter, m
E	enhancement factor, -
Ha	Hatta number, -
K	gas-side overall mass transfer coefficient, m s^{-1}
k	individual mass transfer coefficient, m s^{-1}
k	reaction rate constant, m^3 mol^{-1} s^{-1}
l	membrane length, m
m	dimensionless Henry's constant, -
N	molar CO_2 flux, mol m^{-2} s^{-1}
n	number of membrane fibers, -
$\dot{n}$	molar flow rate, mol/s
Re	Reynolds number, -
Sc	Schmidt number, -
Sh	Sherwood number, -
$\dot{V}$	volumetric flow rate, m^3 s^{-1}
v	superficial velocity, m s^{-1}
α	CO_2 loading in absorbent, mol mol^{-1}
ΔC_m	logarithmic mean driving force, -
δ	membrane thickness, m
ε	membrane porosity, -

η efficiency, %

ν kinematic viscosity, $m^2\ s^{-1}$

τ membrane tortuosity, -

Subscripts

1 forward reaction

-1 reverse reaction

abs absorption

B base

c contactor

chem chemical

des desorption

eff effective (diffusivity)

G gas

i inside (membrane fiber)

in inlet to the membrane module

L liquid

LM liquid-membrane interface

M membrane

o outside (membrane fiber)

out outlet from the membrane module

phys physical

PG potassium glycinate

R reaction

∞ limiting (enhancement factor)

6. References

[1] M. Mikkelsen, M. Jørgensen and F. C. Krebs, "The teraton challenge. A review of fixation and transformation of carbon dioxide.," *Energy Environ. Sci.,* vol. 3, p. 43–81, 2010.

[2] J. Wilcox, Carbon Capture, New York: Springer Science+Business Media, LLC, 2012.

[3] M. Peters, B. Köhler, W. Kuckshinrichs, W. Leitner, P. Markewitz and T. E. Müller, "Chemical Technologies for Exploiting and Recycling Carbon Dioxide into the Value Chain," *ChemSusChem,* vol. 4, p. 1216 – 1240, 2011.

[4] N. MacDowell, N. Florin, A. Buchard, J. Hallett, A. Galindo, G. Jackson, C. S. Adjiman, C. K. WIlliams, N. Shah and P. Fennell, "An overview of CO_2 capture technologies," *Energy Environ. Sci.,* vol. 3, p. 1645–1669, 2010.

[5] E. S. Rubin, H. Mantripragada, A. Marks, P. Versteeg and J. Kitchin, "The outlook for improved carbon capture technology," *Prog. Energy Combust. Sci.,* vol. 38, pp. 630-671, 2012.

[6] M. E. Boot-Handford, J. C. Abanades, E. J. Anthony, M. J. Blunt, S. Brandani, N. Mac Dowell, J. R. Fernández, M.-C. Ferrari, R. Gross, J. P. Hallett, R. S. Haszeldine, P. Heptonstall, A. Lyngfelt, Z. Makuch, E. Mangano and R. T. J. Porter, "Carbon capture and storage update," *Energy Environ. Sci.,* vol. 7, pp. 130-189, 2014.

[7] B. Dutcher, M. Fan and A. G. Russell, "Amine-Based CO_2 Capture Technology Development from the Beginning of 2013 - A Review," *ACS Appl. Mater. Interfaces,* vol. 7, p. 2137−2148, 2015.

[8] K. A. Mumford, Y. Wu, K. H. Smith and G. W. Stevens, "Review of solvent based carbon-dioxide capture technologies," *Front. Chem. Sci. Eng.,* vol. 9, no. 2, pp. 125-141, 2015.

[9] M. Ramdin, T. W. de Loos and T. J. H. Vlugt, "State-of-the-Art of CO_2 Capture with Ionic Liquids," *Ind. Eng. Chem. Res.,* vol. 51, p. 8149−8177, 2012.

[10] D. M. D'Alessandro, B. Smit and J. R. Long, "Carbon Dioxide Capture: Prospects for New Materials," *Angew. Chem. Int. Ed.,* vol. 49, p. 6058 – 6082, 2010.

[11] A. Brunetti, F. Scura, G. Barbieri and E. Drioli, "Membrane technologies for CO_2 separation," *J. Membr. Sci.,* vol. 359, p. 115–125, 2010.

[12] A. Gabelman and S.-T. Hwang, "Hollow fiber membrane contactors," *J. Membr. Sci.,* vol. 159, no. 1-2, pp. 61-106, 1999.

[13] S. Zhao, P. H. M. Feron, L. Deng, E. Favre, E. Chabanon, S. Yan, J. Hou, V. Chen and H. Qi, "Status and progress of membrane contactors in post-combustion carbon capture: A state-of-the-art review of new developments," *J. Membr. Sci.,* vol. 511, pp. 180-206, 2016.

[14] E. Cussler, "Hollow fiber contactors," in *Membrane Processes in Separation and Purification*, Netherlands, Kluwer Academic Publishers, 1994, pp. 375-394.

[15] E. Favre and H. F. Svendsen, "Membrane contactors for intensified post-combustion carbon dioxide capture by gas–liquid absorption processes," *J. Membr. Sci.,* Vols. 407-408, pp. 1-7, 2012.

[16] S. Mosadegh-Sedghi, D. Rodrigue, J. Brisson and M. C. Iliuta, "Wetting phenomenon in membrane contactors – Causes and prevention," *J. Membr. Sci.,* vol. 452, pp. 332-353, 2014.

[17] E. Chabanon, D. Roizard and E. Favre, "Membrane Contactors for Postcombustion Carbon Dioxide Capture: A Comparative Study of Wetting Resistance on Long Time Scales," *Ind. Eng. Chem. Res.,* vol. 50, no. 13, pp. 8237-8244, 2011.

[18] Y. Lv, X. Yu, S.-T. Tu, J. Yan and E. Dahlquist, "Wetting of polypropylene hollow fiber membrane contactors," *J. Membr. Sci.,* vol. 362, no. 1-2, pp. 444-452, 2010.

[19] D. deMontigny, P. Tontiwachwuthikul and A. Chakma, "Using polypropylene and polytetrafluoroethylene membranes in a membrane contactor for CO_2 absorption," *J. Membr. Sci.,* vol. 277, pp. 99-107, 2006.

[20] P. S. Kumar, J. A. Hogendoorn, P. H. M. Feron and G. F. Versteeg, "New absorption liquids for the removal of CO_2 from dilute gas streams using membrane contactors," *Chem. Eng. Sci.,* vol. 57, no. 9, pp. 1639-1651, 2002.

[21] A. F. Portugal, P. W. J. Derks, G. F. Versteeg, F. D. Magalhães and A. Mendes, "Characterization of potassium glycinate for carbon dioxide absorption purposes," *Chem. Eng. Sci.,* vol. 62, p. 6534 – 6547, 2007.

[22] P. H. M. Feron and A. E. Jansen, "CO_2 separation with polyolefin membrane contactors and dedicated absorption liquids: performances and prospects," *Sep. Purif. Technol.,* vol. 27, p. 231–242, 2002.

[23] P. S. Kumar, J. A. Hogendoorn and G. F. Versteeg, "Kinetics of the reaction of CO2 with aqueous potassium salt of taurine and glycine," *AIChE J.,* vol. 49, no. 1, pp. 203-213, 2003.

[24] S. Yan, M.-X. Fang, W.-F. Zhang, S.-Y. Wang, Z.-K. Xu, Z.-Y. Luo and K.-F. Cen, "Experimental study on the separation of CO_2 from flue gas using hollow fiber membrane contactors without wetting," *Fuel Process. Technol.,* vol. 88, pp. 501-511, 2007.

[25] J.-G. Lu, Y.-F. Zheng and M.-D. Cheng, "Membrane contactor for CO_2 absorption applying amino-acid salt solutions," *Desalination,* vol. 249, p. 498–502, 2009.

[26] O. Falk-Pedersen and H. Dannström, "Separation of carbon dioxide from offshore gas turbine exhaust," *Energy Convers. Mgmt,* vol. 38, pp. S81-S86, 1997.

[27] O. Falk-Pedersen, M. Grønvold, P. Nøkleby and F. Bjerve, "CO_2 capture with membrane contactors," *Int. J. Green Energy,* vol. 2, p. 157–165, 2005.

[28] S.-H. Yeon, K.-S. Lee, B. Sea, Y.-I. Park and K.-H. Lee, "Application of pilot-scale membrane contactor hybrid system for removal of carbon dioxide from flue gas," *J. Membr. Sci.,* vol. 257, p. 156–160, 2005.

[29] P. Kosaraju, A. S. Kovvali, A. Korikov and K. K. Sirkar, "Hollow Fiber Membrane Contactor Based CO_2 Absorption-Stripping Using Novel Solvents and Membranes," *Ind. Eng. Chem. Res.,* vol. 44, pp. 1250-1258, 2005.

[30] C. A. Scholes, A. Qader, G. W. Stevens and S. E. Kentish, "Membrane Gas-Solvent Contactor Pilot Plant Trials of CO_2 Absorption from Flue Gas," *Sep. Sci. Technol.,* vol. 49, p. 2449–2458, 2014.

[31] S. Li, T. J. Pyrzynski, N. B. Klinghoffer, T. Tamale, Y. Zhong, J. L. Aderhold, S. J. Zhou, H. S. Meyer, Y. Ding and B. Bikson, "Scale-up of PEEK hollow fiber membrane contactor for post-combustion CO_2 capture," *J. Membr. Sci.,* vol. 527, pp. 92-101, 2017.

[32] S. Nii, Y. Iwata, K. Takahashi and H. Takeuchi, "Regeneration of CO_2-loaded carbonate solution by reducing pressure," *J. Chem. Eng. Jpn.,* vol. 28, no. 2, pp. 148-153, 1995.

[33] M. Fang, S. Yan, Z. Luo, M. Ni and K. Cen, "CO_2 chemical absorption by using membrane vacuum regeneration technology," *Energy Procedia,* vol. 1, pp. 815-822, 2009.

[34] Z. Wang, M. Fang, Y. Pan, S. Yan and Z. Luo, "Amine-based absorbents selection for CO_2 membrane vacuum regeneration technology by combined absorption–desorption analysis," *Chem. Eng. Sci.,* vol. 93, pp. 238-249, 2013.

[35] S. Yan, M. Fang, Z. Wang and Z. Luo, "Regeneration performance of CO_2-rich solvents by using membrane vacuum regeneration technology: Relationships between absorbent structure and regeneration efficiency," *Appl. Energy,* vol. 98, pp. 357-367, 2012.

[36] H. Nieminen, L. Järvinen, V. Ruuskanen, A. Laari, T. Koiranen and J. Ahola, "Insights into a membrane contactor based demonstration unit for CO_2 capture," *Sep. Purif. Technol.,* vol. 231, 2020.

[37] P. Kumar, J. Hogendoorn, P. Feron and G. Versteeg, "Approximate solution to predict the enhancement factor for the reactive absorption of a gas in a liquid flowing through a microporous membrane hollow fiber," *J. Membr. Sci,* vol. 213, no. 1-2, pp. 231-245, 2003.

[38] J.-L. Li and B.-H. Chen, "Review of CO_2 absorption using chemical solvents in hollow fiber membrane contactors," *Sep. Purif. Technol.,* vol. 41, no. 2, pp. 109-122, 2005.

[39] A. Portugal, P. Derks, G. Versteeg, F. Magalhães and A. Mendes, "Characterization of potassium glycinate for carbon dioxide absorption purposes," *Chem. Eng. Sci.,* vol. 62, p. 6534 – 6547, 2007.

[40] B. M. S. E. H. &. T. K. Lerche, CO_2 Capture from Flue gas using Amino acid salt solutions., Kgs. Lyngby: Technical University of Denmark (DTU), 2012.

[41] A. F. Portugal, J. M. Souda, F. D. Magalhães and A. Mendes, "Solubility of carbon dioxide in aqueous solutions of amino acid salts," *Chem. Eng. Sci.,* vol. 64, pp. 1993-2002, 2009.

[42] P. Kumar, J. Hogendoorn and G. Versteeg, "Kinetics of the reaction of CO_2 with aqueous potassium salt of taurine and glycine," *AIChE J.,* vol. 49, no. 1, pp. 203-213, 2003.

[43] H. Kreulen, C. Smolders, G. Versteeg and W. van Swaaij, "Microporous hollow fibre membrane modules as gas-liquid contactors. Part 1. Physical mass transfer processes - A specific application: Mass transfer in highly viscous liquids," *J. Membr. Sci.,* vol. 78, no. 3, pp. 197-216, 1993.

[44] V. Dindore, D. Brilman and G. Versteeg, "Hollow fiber membrane contactor as a gas–liquid model contactor," *Chem.Eng.Sci.,* vol. 60, no. 2, pp. 467-479, 2005.

[45] M. Yang and E. L. Cussler, "Designing hollow-fiber contactors," *AIChE J.,* vol. 32, pp. 1910-1916, 1986.

[46] C. A. Scholes, S. E. Kentish, G. W. Stevens and D. deMontigny, "Comparison of thin film composite and microporous membrane contactors for CO_2 absorption into monoethanolamine," *Int. J. Greenhouse Gas Control,* vol. 42, pp. 66-74, 2015.

[47] S. Khaisri, D. deMontigny, P. Tontiwachwuthikul and R. Jiraratananon, "Comparing membrane resistance and absorption performance of three different membranes in a gas absorption membrane contactor," *Sep. Purif. Technol.,* vol. 65, p. 290–297, 2009.

[48] S. Rode, P. T. Nguyen, D. Roizard, R. Bounaceur, C. Castel and E. Favre, "Evaluating the intensification potential of membrane contactors for gas absorption in a chemical solvent: A generic one-dimensional methodology and its application to CO_2 absorption in monoethanolamine," *J. Membr. Sci.,* vol. 389, pp. 1-16, 2012.

[49] W. P. M. van Swaaij and G. F. Versteeg, "Mass Transfer Accompanied With Complex Reversible Chemical Reactions In Gas-Liquid Systems: An Overview," *Chem. Eng. Sci.,* vol. 47, pp. 3181-3195, 1992.

[50] H.-Y. Zhang, R. Wang, D. Liang and J. Tay, "Theoretical and experimental studies of membrane wetting in the membrane gas–liquid contacting process for CO_2 absorption," *J. Membr. Sci.,* vol. 308, pp. 162-170, 2008.

[51] J. R. e. Rumble, "Physical Constants of Organic Compounds," in *CRC Handbook of Chemistry and Physics, 100th Edition (Internet Version 2019)*, Boca Raton, CRC Press/Taylor & Francis, 2019.

[52] Y.-S. Kim and S.-M. Yang, "Absorption of carbon dioxide through hollow fiber membranes using various aqueous absorbents," *Sep. Purif. Technol.,* vol. 21, pp. 101-109, 2000.

[53] F. He, T. Wang, M. Fang, Z. Wang, H. Yu and Q. Ma, "Screening Test of Amino Acid Salts for CO_2 Absorption at Flue Gas Temperature in a Membrane Contactor," *Energy Fuels,* vol. 31, p. 770−777, 2017.

[54] J. Franco, D. deMontigny, S. Kentish, J. Perera and G. Stevens, "A Study of the Mass Transfer of CO_2 through Different Membrane Materials in the Membrane Gas Absorption Process," *Sep. Sci. Technol. ,* vol. 43, pp. 225-244, 2008.

[55] S.-H. Yeon, B. Sea, Park, Y.I. and K.-H. Lee, "Determination of Mass Transfer Rates in PVDF and PTFE Hollow Fiber Membranes for CO_2 Absorption," *Sep. Sci. Technol.,* vol. 38, no. 2, pp. 271-293, 2003.

[56] S.-H. Lin, C.-F. Hsieh, M.-H. Li and K.-L. Tung, "Determination of mass transfer resistance during absorption of carbon dioxide by mixed absorbents in PVDF and PP membrane contactor," *Desalination,* vol. 249, pp. 647-653, 2009.

[57] L. Wang, Z. Zhang, B. Zhao, H. Zhang, X. Lu and Q. Yang, "Effect of long-term operation on the performance of polypropylene and polyvinylidene fluoride membrane contactors for CO_2 absorption," *Sep. Purif. Technol.,* vol. 116, pp. 300-306, 2013.

[58] R. Wang, H. Zhang, P. Feron and D. Liang, "Influence of membrane wetting on CO_2 capture in microporous hollow fiber membrane contactors," *Sep. Purif. Technol.,* vol. 46, no. 1-2, pp. 33-40, 2005.

[59] E. Chabanon and E. Roizard. D-: Favre, "Modeling strategies of membrane contactors for post-combustion carbon capture: A critical comparative study," *Chem. Eng. Sci.,* vol. 87, pp. 393-407, 2013.